Journal of Hazardous Materials 219–220 (2012) 283–288

Contents lists available at SciVerse ScienceDirect

Journal of Hazardous Materials

journal homepage: www.elsevier.com/locate/jhazmat

Mechanism of the reduction of hexavalent chromium by organo-montmorillonite supported iron nanoparticles

Pingxiao Wu[a,*], Shuzhen Li[b], Liting Ju[a], Nengwu Zhu[a,c,d], Jinhua Wu[a], Ping Li[a], Zhi Dang[a,c,d]

[a] College of Environmental Science and Engineering, South China University of Technology, Guangzhou 510006, PR China
[b] School of Chemical and Environmental Engineering, Wuyi University, Jiangmen, Guangdong Province 529020, PR China
[c] The Key Lab of Pollution Control and Ecosystem Restoration in Industry Clusters, Ministry of Education, Guangzhou 510006, PR China
[d] The Key Laboratory of Environmental Protection and Eco-Remediation of Guangdong Regular Higher Education Institutions, PR China

ARTICLE INFO

Article history:
Received 20 January 2012
Received in revised form 3 April 2012
Accepted 4 April 2012
Available online 10 April 2012

Keywords:
Zero-valent iron
Nanoparticles
Reduction
Chromium
Groundwater

ABSTRACT

Iron nanoparticles exhibit greater reactivity than micro-sized Fe^0, and they impart advantages for groundwater remediation. In this paper, supported iron nanoparticles were synthesized to further enhance the speed and efficiency of remediation. Natural montmorillonite and organo-montmorillonite were chosen as supporting materials. The capacity of supported iron nanoparticles was evaluated, compared to unsupported iron nanoparticles, for the reduction of aqueous Cr(VI). The reduction of Cr(VI) was much greater with organo-montmorillonite supported iron nanoparticles and fitted the pseudo-second order equation better. With a dose at 0.47 g/L, a total removal capacity of 106 mg Cr/g Fe^0 was obtained. Other factors that affect the efficiency of Cr(VI) removal, such as pH values, the initial Cr(VI) concentration and storage time of nanoparticles were investigated. X-ray photoelectron spectrometry (XPS) and X-ray absorption near edge structure (XANES) were used to figure out the mechanism of the removal of Cr(VI). XPS indicated that the Cr(VI) bound to the particle surface was completely reduced to Cr(III) under a range of conditions. XANES confirmed that the Cr(VI) reacted with iron nanoparticles was completely reduced to Cr(III).

1. Introduction

Iron nanoparticles are very effective for the transformation and detoxification of a wide variety of common environmental contaminants, such as chlorinated organic solvents, organochlorine pesticides, and PCBs [1–4]. The in situ chemical reduction of contaminants by iron nanoparticles represents a potentially more effective, lower cost alternative than other remediation technologies such as pump-and-treat [5], flushing with solvents and surfactants [6], steam treatment [7], and natural attenuation via bio- and phytoremediation [8].

A major challenge for groundwater remediation of reactive nanomaterials is their strong tendency to agglomerate, with rapid sedimentation and consequently limited mobility of the nanoparticles in an aquatic environment. Our previous research on clay minerals supporting iron nanoparticles demonstrated that the presence of montmorillonite and surfactant apparently decreased the extent of aggregation and the size of iron nanoparticles [9].

In this study, Cr(VI) was chosen as a typical and toxic contaminant to evaluate the performance of supported iron nanoparticles. Chromium originates from alloys and steel manufacturing, metal finishing, electroplating, leather tanning, or pigment synthesis and dying [10]. Cr(VI) is considered to be the most toxic form of chromium. It exists in groundwater systems as the oxyanion $H_xCrO_4^{x-2}$ (chromate), which exhibits high water solubility and is a mutagen, teratogen, and carcinogen [11]. Cr(III) is much less mobile and less available for biological uptake, due to the low solubility of Cr(III) hydroxide in water over a wide pH range [12].

Organo-montmorillonite supported iron nanoparticles were tested for their ability to separate and immobilize Cr(VI) from aqueous solution. Comparisons were made between unsupported iron nanoparticles and supported nanoparticles. The reaction mechanisms of the removal of Cr(VI) were involved. In addition, details of the combination of iron nanoparticles and clay mineral layers were further investigated.

2. Experimental

2.1. Chemicals

Montmorillonite (Mont) was purchased from Nanhai, Guangdong province, China. Potassium dichromate ($K_2Cr_2O_7$), ferrous chloride tetrahydrate ($FeCl_2{\cdot}4H_2O$), and hexadecyl trimethyl ammonium bromide [HDTMA, $CH_3(CH_2)_{14}CH_2(CH_3)_3NBr$] were

* Corresponding author. Tel.: +86 20 39380538; fax: +86 20 39383725.
E-mail address: pppxwu@scut.edu.cn (P. Wu).

0304-3894/$ – see front matter © 2012 Elsevier B.V. All rights reserved.
http://dx.doi.org/10.1016/j.jhazmat.2012.04.008

obtained from the Guangzhou Chemical Reagent Factory, China. Sodium borohydride ($NaBH_4$) was from the Tianjin Fuchen chemical reagent factory. All chemicals were obtained in purity >99%and were used as received. All stock solutions were prepared with argon-sparged deionized water.

2.2. Iron nanoparticles

Procedures used in the preparation of HDTMA modified montmorillonite (HDTMA-Mont), iron nanoparticles, and supported iron nanoparticles were reported previously [9]. Briefly, a sample of $FeCl_2{\cdot}4H_2O$ weighing 17,800 g was dissolved in 60 mL solution (20 mL deionized water and 40 mL absolute ethanol). Amounts of 4000 g of Mont or HDTMA-Mont were mixed with the $FeCl_2$ solution on a magnetic stirrer. $NaBH_4$ solution of 1 mol/L was added into the $FeCl_2$ solution. Black iron particles were separated from the mixture by vacuum filtration and washed with 99% ethanol. Samples were dried in a vacuum desiccator. Montmorillonite and HDTMA modified montmorillonite supported iron nanoparticles were noted as Mont/iron and HDTMA-Mont/iron, respectively.

2.3. Batch experiments

2.3.1. Comparisons of various materials

A solution of 50 mg/L of Cr(VI) was prepared by dissolving appropriate amounts of $K_2Cr_2O_7$ in deionized water. The Fe^0 mass fraction of unsupported iron, Mont/iron and HDTMA-Mont/iron nanoparticles were 89.6, 60.5 and 52.2%, respectively. To test the effect of total Cr concentrations on the reduction reaction, an amount of each material containing 0.100 g of Fe^0 (0.117 g of unsupported iron nanoparticles, 0.165 g of Mont/iron, and 0.192 g of HDTMA-Mont/iron) was added into 300 mL of 50 mg/L Cr(VI) solution. The initial pH of the Cr(VI) solution was 5.0 without the addition of buffers. Each bottle was shaken laterally in a water bath shaker with a rate of 150 rpm at room temperature. After the desired reaction time, samples were taken with a 10 mL syringe, and filtered through a 0.2 μm polyethersulfone (PES) filter (Membrana, Germany). Total chromium was determined by atomic absorption (AA) spectroscopy. The Cr(VI) concentration was analyzed using the diphenylcarbohydrazide method and measured with a ultraviolet and visible spectrophotometer (UV2450, Shimadzu, Japan) [13]. This method is insensitive to Cr(III). The average value of Cr(VI) concentration was calculated from two identical sample analyses.

2.3.2. Experimental factors in the reduction of Cr(VI)

Some factors affecting the reduction of HDTMA-Mont/iron were investigated. Experiments were carried out with the procedure and under the same conditions as described in Section 2.3.1, except as follows. Initial solution pH values between 4.0 and 8.0 adjusted using 0.1 M HCl or 0.1 M NaOH were studied. Corresponding to the addition of 0.08, 0.10, 0.12, 0.14 and 0.16 g Fe^0/L, the amount of HDTMA-Mont/iron should be 0.27, 0.33, 0.40, 0.47 and 0.53 g/L, respectively. The effect of Cr(VI) concentration was considered by using solution containing Cr(VI) at concentrations of 30, 40, 50 and 60 mg/L. In order to evaluate the stability of HDTMA-Mont/iron, reduction rates of fresh sample and the same sample preserved by argon after 15 days were observed.

2.4. Characterization with X-ray diffraction (XRD)

XRD analysis was undertaken using a D8 Discover (Bruker, Germany) instrument and Cu-K_α radiation (λ = 1.54 Å). Specimens were prepared for XRD analysis by sedimenting dispersion on a zero-background slide and analyzed in ambient air. Continuous scans from 1° to 60° 2θ were collected at a scan rate of about 1° 2θ min^{-1}.

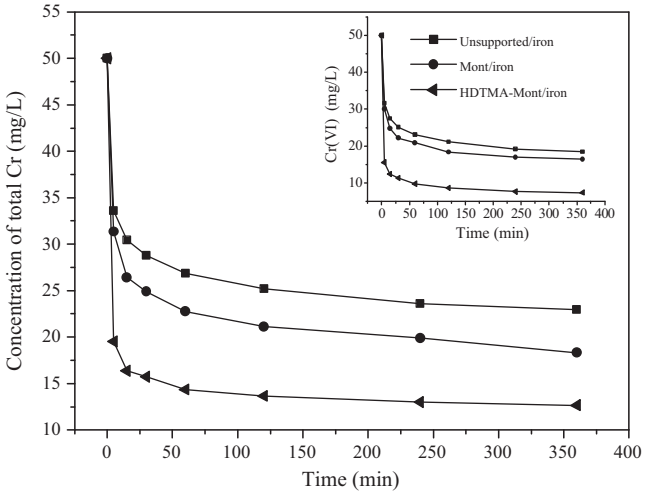

Fig. 1. Disappearance of total chromium and Cr(VI) in the presence of unsupported and supported iron nanoparticles. Reactor contained 0.100 g of Fe^0 and an initial Cr(VI) concentration of 50 mg/L. The initial pH was 5.0 without added buffers.

2.5. X-ray photoelectron spectrometer (HR-XPS)

The X-ray photoelectron spectra were measured with an ANELVA AES-430S X-ray photoelectron spectrometer and the binding energy of C 1s was shifted to 284.6 eV as an internal reference. The powder was sprinkled onto the surface of sticky carbon tape for analysis. The pass energy was 50 eV and a conventional Al Kα (1486.7 eV) anode radiation source was used as the excitation source.

2.6. X-ray absorption near edge structure (XANES) spectroscopy

Cr K-edge XANES measurements were conducted at the Beam line 14W1 of the Shanghai Synchrotron Radiation Facility in Shanghai, China. The K-edge XANES scans for Cr (5864–6051 eV) were recorded with step increments of 0.5 eV controlled with a Si(1 1 1) monochromator. The scans for each sample were averaged, followed by background removal and normalization. The spectra of pure Cr_2O_3, $CrCl_3$ and K_2CrO_4 chemicals were also obtained to serve as the reference standards for the Cr(III) and Cr(VI) oxidation states.

3. Results and discussion

3.1. Kinetic of the reduction of Cr(VI) by iron nanoparticles

Results in Fig. 1 show that HDTMA-Mont/iron reduced the greatest amount of chromium, from 50 to 12 mg/L within 6 h, whereas the unsupported iron nanoparticles removed the least amount. The presence of montmorillonite and surfactant effectively decreased the extent of aggregation and the size of individual iron particles [9]. Morphology differences between supported and unsupported iron nanoparticles were the reason for the higher activity, especially when these particles were well distributed on the surface of organo-montmorillonite. There are two main mechanisms for the removal of total chromium. First, an adsorption phase existed during the first 30 min, and the total chromium concentration decreased rapidly with time. It is suggested that the mechanism is physical (i.e., that it involved occlusion of the zero-valent iron) rather than chemical [14,15]. The second phase is that Cr(VI) was reduced and precipitated by the increase in pH ultimately. The

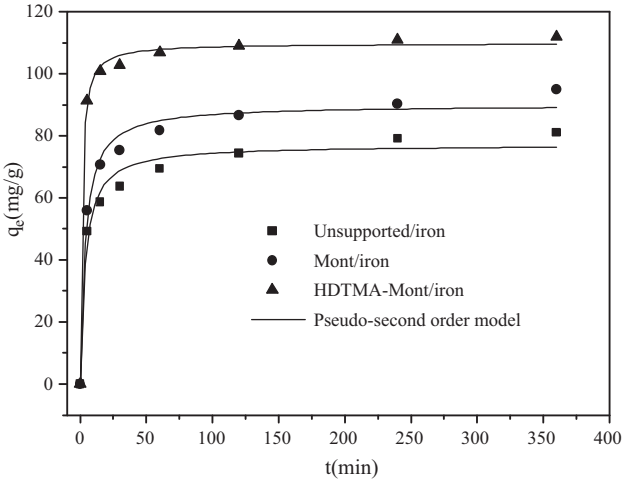

Fig. 2. Pseudo-second-order plot for the removal of Cr(VI) on the various materials.

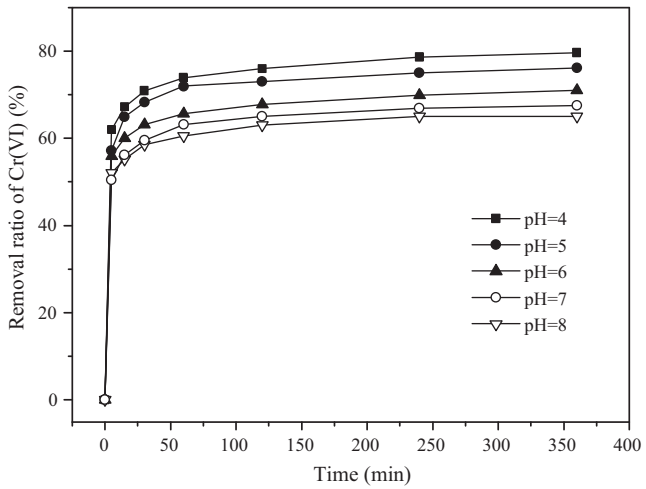

Fig. 3. Removal rate of Cr(VI) in the aqueous phase at various pH values as a function of time. The initial Cr(VI) concentrations was 50 mg/L. The Fe^0 dose of HDTMA-Mont/iron was 0.33 g/L.

initial pH value of Cr(VI) was 5.0 and rose to 8.0–9.0 after the contact with iron nanoparticles. In the pH range of 8–9, precipitation of Cr(III) could be the cause of decrease of total chromium from solution. $Cr(OH)_3{}^0$ was reported to dominate for pH between about 6.5 and 10.5 [12].

In order to investigate the mechanism of reduction and potential rate-controlling steps such as mass transport and chemical reaction processes, kinetic models were used to test experimental data. The pseudo-first-order and pseudo-second-order model were used to fit the experimental data.

The pseudo-first-order rate expression of Lagergren model is generally expressed as follows:

$$\ln(q_e - q_t) = \ln q_e - K_1 t \quad (1)$$

where q_t and q_e are the amount of Cr(VI) adsorbed per unit mass (mg/g) at any time (t) and at equilibrium, respectively. The K_1 is the rate constant of first-order adsorption.

The kinetics of the removal process shown in Fig. 2 was simulated using the pseudo-second-order model with the rate expression given by:

$$\frac{t}{q_t} = \frac{1}{k_p q_e^2} + \frac{t}{q_e} \quad (2)$$

where k_p is the second order rate constant (g/mg min), as presented in Fig. 2, the sorption of Cr(VI) onto iron nanoparticles fits the pseudo-second order model quite well, since the correlation coefficients (R) for q_e against time from the pseudo-second order rate law are greater than 0.97 for three materials (Table 1). The pseudo-first-order equation does not fit well for the whole range of contact time and is generally applicable over the initial 20–30 min of the sorption process. This result indicates that this sorption system is a pseudo-second-order reaction, implying the rate-limiting step may be a chemical sorption involving valency forces through sharing or exchanging of electrons between sorbent and sorbate.

Table 1
Kinetics constants for the removal of Cr(VI) on the various materials.

Sample	Pseudo-second-order model			Pseudo-first-order model
	R^2	q_e	k_p	R^2
Unsupported/iron	0.975	77.1	0.00358	0.589
Mont/iron	0.984	90.9	0.00303	0.612
HDTMA-Mont/iron	0.997	109.9	0.00828	0.643

3.1.1. Influence of pH

The efficiency of Cr(VI) reduction by HDTMA-Mont/iron decreased with increasing solution pH (Fig. 3). Cr(VI) existed as $CrO_4{}^{2-}$, $HCrO_4{}^-$, H_2CrO_4, $HCr_2O_7{}^-$, or $Cr_2O_7{}^{2-}$, depending on the pH of the medium and the total Cr(VI) concentration [16]. In low pH solutions, $HCrO_4{}^-$ was the prevalent form of hexavalent chromium, which subsequently shifted to $CrO_4{}^{2-}$ and $Cr_2O_7{}^{2-}$ as the pH was increased. Low acidic conditions also caused the surface of the nanoparticles to be protonated to a higher extent, which resulted in a strong attraction between the negatively charged Cr(VI) complex ions and the positively charged surface [17].

Zero-valent iron (Fe^0) is a moderate reducing reagent, which can react with dissolved oxygen and to some extent with water [18]:

$$2Fe^0 + 4H^+ + O_2 \rightarrow 2Fe^{2+} + 2H_2O \quad (3)$$

$$Fe^0 + 2H_2O \rightarrow Fe^{2+} + H_2 + 2OH^- \quad (4)$$

Reduction of Cr(VI) under acidic conditions is attributed to the following:

$$Fe^{2+} + H_2CrO_4 + H^+ \rightarrow Fe^{3+} + H_3CrO_4 \quad (5)$$

$$Fe^{2+} + H_3CrO_4 + H^+ \rightarrow Fe^{3+} + H_4CrO_4 \quad (6)$$

$$Fe^{2+} + H_4CrO_4 + H^+ \rightarrow Fe^{3+} + Cr(OH)_3 + H_2O \quad (7)$$

To simplify the process, the reaction of Cr(VI) reduced by iron nanoparticles is presented as:

$$2CrO_4{}^{2-} + 3Fe^0 + 10H^+ \rightarrow 2Cr(OH)_3 + 3Fe^{2+} + 2H_2O \quad (8)$$

The iron oxidation and Cr(VI) reduction reactions are favored at low pH (Eqs. (3)–(8)). Moreover, the effect of pH on the reduction Cr(VI) might be influenced not only by H^+ consumption in the overall reaction (Eq. (8)) and iron geochemistry but also by the relatively low solubility of Cr(III) oxides and mixed chromium(III)/iron(III) oxides [19].

3.1.2. Influence of HDTMA-Mont/iron dosage

The influence of nanoparticles dosage on Cr(VI) reduction was examined at dosages between 0.27 and 0.53 g/L. The residual Cr(VI) was apparently a function of the applied Fe^0 dose (Fig. 4a): the higher the Fe^0 concentration, the lower the residual chromium in solution. An Fe^0 concentration of 0.47 g/L was able to reduce Cr(VI) completely. An increase in nanoparticle concentration generally increased the number of binding sites, which in turn increased the reduction of Cr(VI). The uptake is a measure of the amount

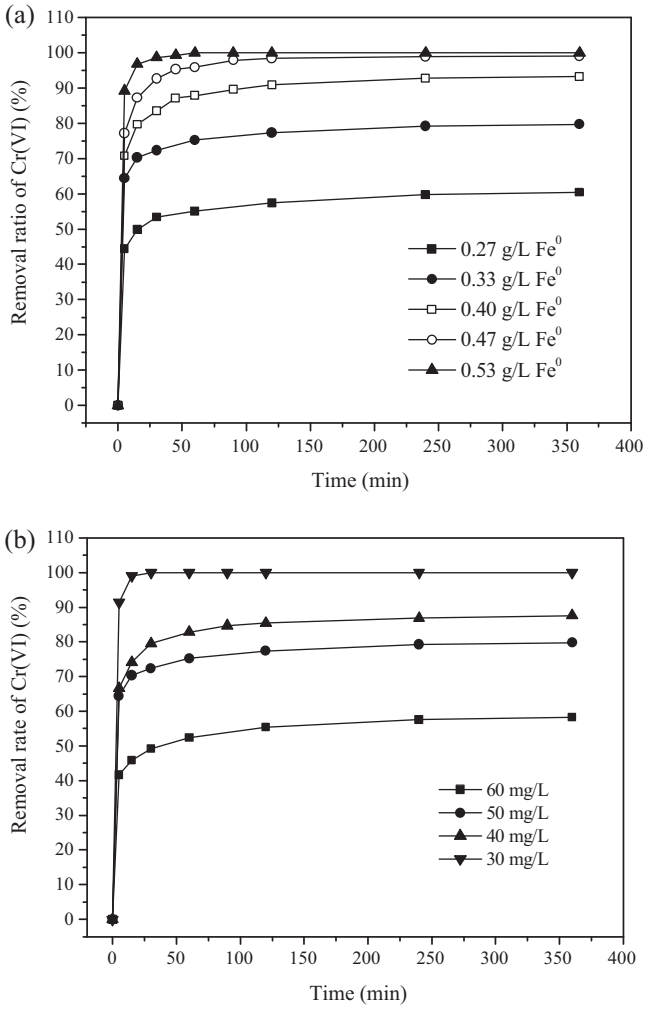

Fig. 4. Removal rate of Cr(VI) in the aqueous phase at (a) various Fe^0 dosage and (b) initial concentration as a function of time. The Fe^0 dose of HDTMA-Mont/iron was 0.33 g/L. The initial pH was 5.0 without the addition of buffers.

of Cr(VI) ions bound by unit weight of material, its magnitude decreased with the increase in HDTMA-Mont/iron dose. With a dose at 0.47 g/L, a total removal capacity of approximately 106 mg Cr/g Fe^0 was obtained. The dependence of the removal percentage on initial Cr(VI) concentration was reported in Fig. 4b. The extent of Cr(VI) removal was lower when the initial Cr(VI) concentration was high. During the redox reaction, Fe^0 is primarily oxidized to Fe(III) and Cr(VI) was reduced to Cr(III). When both Cr(III) and Fe(III) were in proximity, a thin film of Fe(III)–Cr(III) hydroxides was formed on the Fe^0 nanoparticle surface [20]. The film is believed to increase the resistance for the electron transfer from Fe^0 to Cr(VI) and thus to retard the reduction of Cr(VI) to Cr(III). Li et al. confirmed that the actual Fe–Cr surface structure was a mixture of $Cr_{0.667}Fe_{0.333}OOH$ and $(Cr_{0.667}Fe_{0.333})(OH)_3$ [21]. During the reduction of Cr(VI) by acidic Fe(II)(aq), the surface solid was a composite of $(Fe_{0.75}Cr_{0.25}(OH)_3)$ [22]. The reactivity of sites on zero valent iron may be expected to decline with increasing oxidant concentration. This can be attributed to the effect of potential on the rate of electrochemical reactions and on the passivating effect of a corrosion inhibitor like chromate.

3.1.3. Stabilization of HDTMA-Mont/iron

Under the same conditions, HDTMA-Mont/iron stored for 15 days was less active than a fresh sample. The removal ratio decreased from 79 to 73%. The decreasing efficiency with time

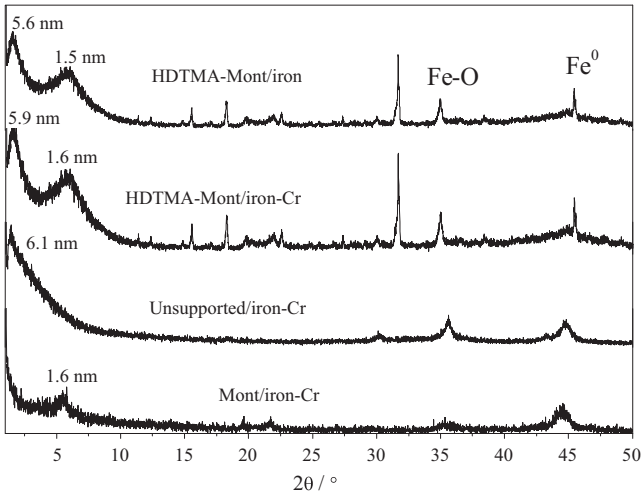

Fig. 5. Powder X-ray diffraction patterns of iron nanoparticles before and after reacting with 50 mg/L Cr (VI).

suggested ongoing oxidation and corrosion to Fe(III) oxide/hydroxide. The amount of oxygen on iron surfaces increases [21]. Lepidocrocite and magnetite/maghemite could be found in iron nanoparticles after 7 days [23,24].

3.2. Structure analysis by powder X-ray diffraction (XRD)

After reacting with 50 mg/L Cr(VI) for 6 h, the XRD pattern of HDTMA-Mont/iron was not significantly changed (Fig. 5). Fe^0 mostly (peak position at 2θ of 45°) and iron oxide crystalline phases (peak position at 2θ of 35° and 32°) were detected. Two reflections appeared at 1° and 5° (Fig. 5), the first of which corresponds to large *d*-spacing and the second is attributed to the (0 0 1) reflection of montmorillonite, as with Mont/iron. Clinard et al. and Yuan et al. concluded the large *d*-spacing reflected the existence of a highly correlated porous structure [25,26], as observed in some ordered porous solids such as Vycor glass and mesoporous silica molecular sieves [27].

Based on our previous research in the structure of supported iron nanoparticles with transmission electron microscope [9], the structure combining montmorillonite and iron nanoparticles was illustrated in Fig. 6. The iron nanoparticles were accommodated by the clay interlayer spaces, which were helpful to protect the nanoparticles from aggregating. This ordered porous structure

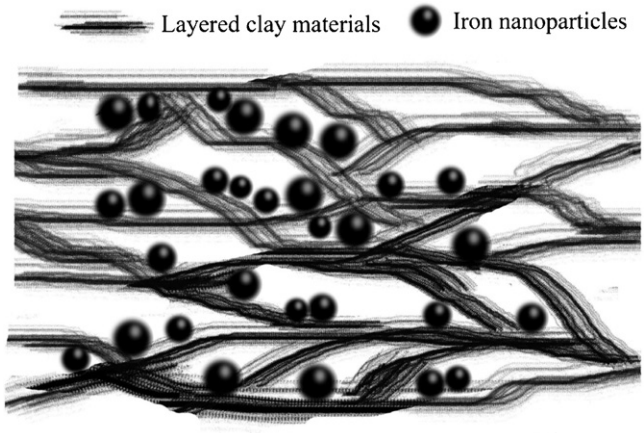

Fig. 6. Schematic representation of the sectional structure of the clay minerals supported iron nanoparticles.

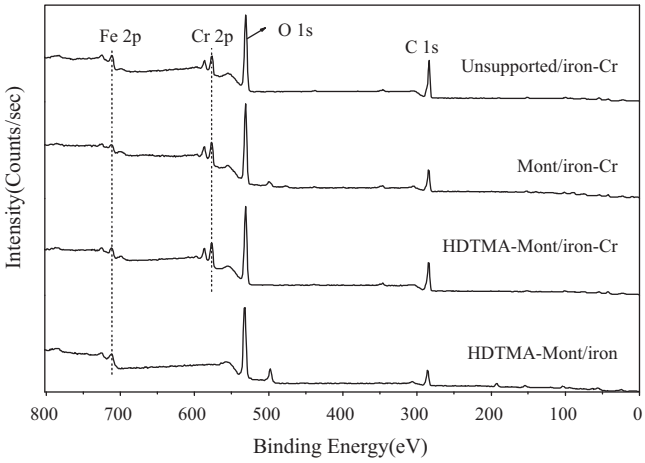

Fig. 7. XPS survey for iron nanoparticles before and after reacting with 50 mg/L Cr (VI).

related to the large *d*-spacing at 1° was resulted from the three-dimensional co-aggregation of clay platelets and iron hydroxyl cations or iron oxide nanoparticles [28]. And the large *d*-spacing was also found in the unsupported iron nanoparticles (Fig. 5).

While Cr(VI) was reduced by Fe^0, low solubility Cr(III) oxides and mixed chromium(III)/iron(III) oxides were formed subsequently [20,29,30]. The first *d*-spacing of HDTMA-Mont/iron was enlarged after the contact with Cr(VI) (Fig. 5), which can be attributed to mixed chromium(III)/iron(III) oxides formed in the process of reaction.

3.3. Characterization with X-ray photoelectron spectrometer (HR-XPS)

Fig. 7 presents a whole-region scan of iron nanoparticles before and after being exposed to a solution containing 50 mg/L Cr(VI). For fresh HDTMA-Mont/iron, the principal elements at the surface are oxygen (40–45%), iron (1–3%), carbon (30–35%), and boron (10–15%). After contact with Cr(VI) for 6 h, new peaks around 580 eV emerge, which are attributed to the photoelectron peaks of chromium and indicate the uptake of chromium on the iron nanoparticle surface [31]. The mass fractions of Cr on the surface of HDTMA-Mont/iron, Mont/iron and iron nanoparticles were 19, 18, and 14%, respectively. The carbon peaks on the surface of Mont/iron and iron nanoparticles were likely due to hydrocarbon and/or carbon dioxide contamination during particle synthesis, sample preparation and transfer [21].

A detailed XPS survey of the regions for chromium 2p was carried out to elucidate the speciation of adsorbed chromium in Fig. 8(a). The chromium spectra had two main peaks, corresponding to $2p_{3/2}$ and $2p_{1/2}$ core levels of chromium. The main $2p_{3/2}$ peaks were located at a binding energy of ~577 eV, which corresponds to Cr(III), based on values ranging between 577.0 and 578.0 eV for $Cr2p_{3/2}$ reported for Cr(III)-containing materials [21,30,32]. The $Cr2p_{1/2}$ signal located at 586.7 eV also supports the existence of Cr(III). Cr(VI) species like CrO_3 were characterized by higher binding energies; 580.0–580.5 eV and 589.0–590.0 eV, since the hexavalent form draws electrons more strongly than the trivalent form [32]. This demonstrates that the Cr(VI) species were indeed reduced by iron nanoparticles and that the adsorbed species were in the form of Cr(III) on the surface of material, whether or not the iron nanoparticles were supported.

The photoelectron peak for the oxygen 1 s region in Fig. 8(b) can be decomposed into three curves, with peaks at ~529, ~531, and ~533 eV, which represent the binding energies of oxygen in

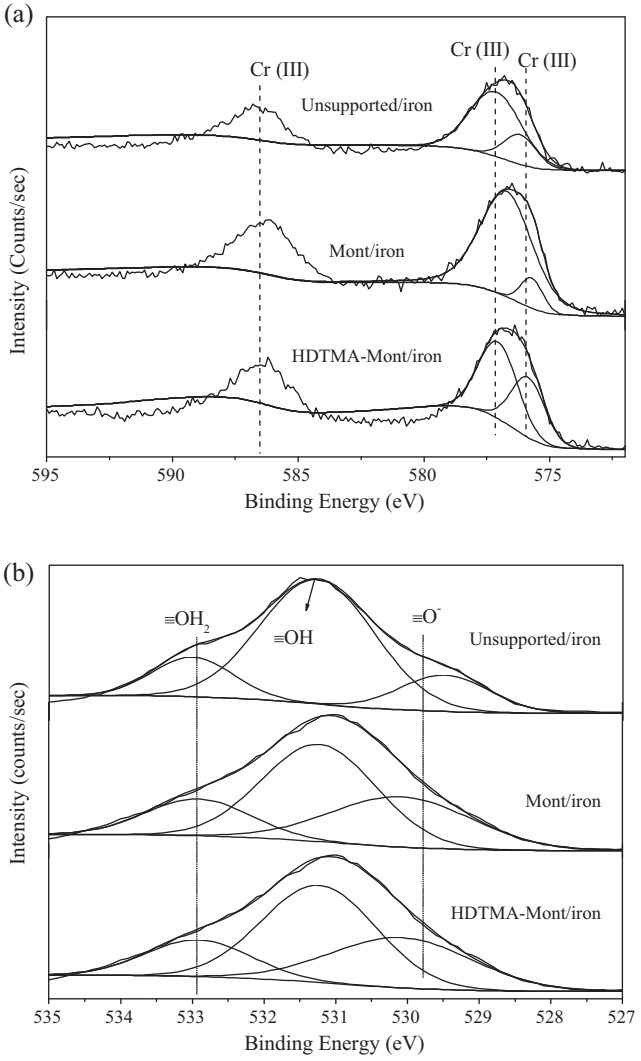

Fig. 8. High-resolution XPS survey of (a) chromium 2p and (b) oxygen 1s of iron nanoparticles after reacting with 50 mg/L Cr (VI).

≡OH, ≡O–, and chemically or physically adsorbed water ($\equiv OH_2$), respectively [21]. Most studies of Cr(VI) reduction by Fe(II)-bearing minerals and by zerovalent iron reported (surface) precipitation of Cr(III)–Fe(III) (hydr)oxides [20,29,30]. This is supported by the O 1s survey, with a high proportion of hydroxides. XPS scans for both Cr_2O_3 and $Cr(OH)_3$ with the former exhibiting a sharp peak at ~530 eV for ≡O– and a smaller one at ~532 eV for the adsorbed H_2O [33]. In contrast, $Cr(OH)_3$ has a peak centering at ~531 eV for OH, as shown in Fig. 8b. This suggests that the Cr(III) compound formed at the surface of the nanoparticles is $Cr(OH)_3$ rather than Cr_2O_3.

3.4. XANES analysis

Normalized Cr K-edge XANES (Fig. 9) were collected for K_2CrO_4, Cr(III) compounds and iron nanoparticles and HDTMA-Mont/iron after reaction with Cr(VI). The K_2CrO_4, $CrCl_3$ and Cr_2O_3 were employed in our study as references to facilitate analysis of the structure of Cr in the Cr(VI)-treated iron nanoparticles. The CrO_4^{2-} tetrahedron, which lacks an inversion center, exhibits a preedge peak at 5995 eV [29,34]. The absence of preedge peak in HDTMA-Mont/iron-Cr was evidence of Cr(VI) reduction to lower oxidation state Cr compounds. Manning et al. reported the XANES analysis of Cr(VI)-treated iron nanoparticles have the same Cr oxidation state

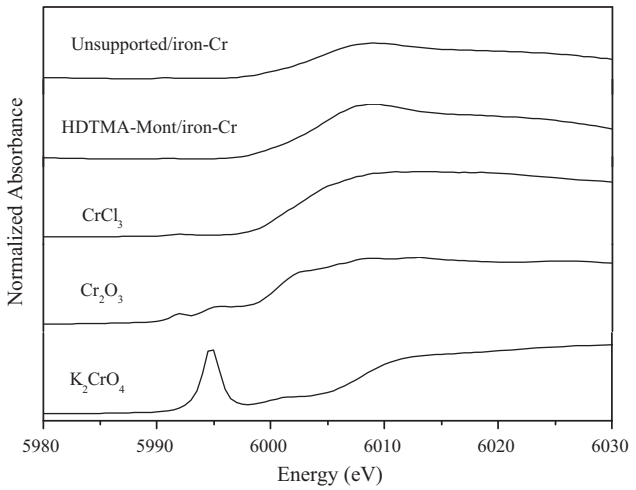

Fig. 9. Normalized Cr K-edge XANES for K_2CrO_4, Cr(III) compounds and iron nanoparticles after reacting with K_2CrO_4 solution.

and nearly identical Cr electronic environment as Cr(III)-treated iron nanoparticles [35].

4. Conclusions

Organo-montmorillonite supported iron nanoparticles were found to be more efficient in the removal of Cr(VI) than unsupported iron nanoparticles. The reaction ratio was accelerated by increase in acidity and iron loading. Increases in the initial Cr(VI) concentration and storage period of nanoparticles caused decrease in the reaction ratio. The structure of the supported iron nanoparticles was stable in the reaction with Cr(VI). HR-XPS and XANES revealed that Cr(VI) was reduced to Cr(III). The HDTMA-Mont/iron and unsupported iron nanoparticles reacted with Cr(VI) in the same mechanism.

Acknowledgements

This work was financially supported by the Program for National Science Foundation of China (Grant No. 41073058, 40973075), Research Fund for the Doctoral Program of Higher Education of China (No. 20100172110028), Science and Technology Plan of Guangdong Province, China (Grant Nos. 2006B36601004, 2008B30302036), Natural Science Foundation of Guangdong Province, China (Grant Nos. 06025666, 9351064101000001). The EXAFS work was performed and supported by BL14W1, Shanghai Synchrotron Radiation Facility (SSRF), China.

References

[1] C.B. Wang, W.X. Zhang, Synthesizing nanoscale iron particles for rapid and complete dechlorination of TCE and PCBs, Environ. Sci. Technol. 31 (1997) 2154–2156.
[2] J. Gotpagar, S. Lyuksyutov, R. Cohn, E. Grulke, D. Bhattacharyya, Reductive dehalogenation of trichloroethylene with zero-valent iron: surface profiling microscopy and rate enhancement studies, Langmuir 15 (1999) 8412–8420.
[3] Y.Q. Liu, S.A. Majetich, R.D. Tilton, D.S. Sholl, G.V. Lowry, TCE dechlorination rates, pathways, and efficiency of nanoscale iron particles with different properties, Environ. Sci. Technol. 39 (2005) 1338–1345.
[4] C.J. Liao, T.L. Chung, W.L. Chen, S.L. Kuo, Treatment of pentachlorophenol contaminated soil using nano-scale zero-valent iron with hydrogen peroxide, J. Mol. Catal. A: Chem. 265 (2007) 189–194.
[5] D.M. Mackay, J.A. Cherry, Groundwater contamination: pump and treat remediation, Environ. Sci. Technol. 23 (1989) 630–636.
[6] J.H. Harwell, D.A. Sabatini, R.C. Knox, Surfactants for ground water remediation, Colloids Surf. A: Physicochem. Eng. Aspects 151 (1999) 255–268.
[7] J. Merino, V. Bucal, Effect of temperature on the release of hexadecane from soil by thermal treatment, J. Hazard. Mater. 143 (2007) 455–461.
[8] G.F. Slater, B.S. Lollar, B.E. Sleep, E.A. Edwards, Variability in carbon isotopic fractionation during biodegradation of chlorinated ethenes: implications for field applications, Environ. Sci. Technol. 35 (2001) 901–907.
[9] S. Li, P. Wu, H. Li, N. Zhu, P. Li, J. Wu, X. Wang, Z. Dang, Synthesis and characterization of organo-montmorillonite supported iron nanoparticles, Appl. Clay Sci. 50 (2010) 330–336.
[10] N. Shevchenko, V. Zaitsev, A. Walcarius, Bifunctionalized mesoporous silicas for Cr(VI) reduction and concomitant Cr(III) immobilization, Environ. Sci. Technol. 42 (2008) 6922–6928.
[11] M. Costa, C.B. Klein, Toxicity and carcinogenicity of chromium compounds in humans, Crit. Rev. Toxicol. 36 (2006) 155–163.
[12] D. Rai, B.M. Sass, D.A. Moore, Chromium(III) hydrolysis constants and solubility of chromium(III) hydroxide, Inorg. Chem. 26 (1987) 345–349.
[13] B.R. James, J.C. Petura, R.J. Vitale, G.R. Mussoline, Hexavalent chromium extraction from soils: a comparison of five methods, Environ. Sci. Technol. 29 (1995) 2377–2381.
[14] S.M. Ponder, J.G. Darab, T.E. Mallouk, Remediation of Cr(VI) and Pb(II) aqueous solutions using supported, nanoscale zero-valent iron, Environ. Sci. Technol. 34 (2000) 2564–2569.
[15] B. Geng, Z. Jin, T. Li, X. Qi, Preparation of chitosan-stabilized Fe^0 nanoparticles for removal of hexavalent chromium in water, Sci. Total. Environ. 407 (2009) 4994–5000.
[16] D. Park, Y.S. Yun, C.K. Ahn, J.M. Park, Kinetics of the reduction of hexavalent chromium with the brown seaweed ecklonia biomass, Chemosphere 66 (2007) 939–946.
[17] S.K. Prabhakaran, K. Vijayaraghavan, R. Balasubramanian, Removal of Cr(VI) ions by spent tea and coffee dusts: reduction to Cr(III) and biosorption, Ind. Eng. Chem. Res. 48 (2009) 2113–2117.
[18] W.X. Zhang, Nanoscale iron particles for environmental remediation: an overview, J. Nanopart. Res. 5 (2003) 323–332.
[19] B.M. Sass, D. Rai, Solubility of amorphous chromium(III)–iron(III) hydroxide solid solutions, Inorg. Chem. 26 (1987) 2228–2232.
[20] R.M. Powell, R.W. Puls, S.K. Hightower, D.A. Sabatini, Coupled iron corrosion and chromate reduction: mechanisms for subsurface remediation, Environ. Sci. Technol. 29 (1995) 1913–1922.
[21] X.Q. Li, J. Cao, W.X. Zhang, Stoichiometry of Cr(VI) immobilization using nanoscale zerovalent iron (nZVI): a study with high-resolution X-ray photoelectron spectroscopy (HR-XPS), Ind. Eng. Chem. Res. 47 (2008) 2131–2139.
[22] I.J. Buerge, S.J. Hug, Influence of mineral surfaces on chromium(VI) reduction by iron(II), Environ. Sci. Technol. 33 (1999) 4285–4291.
[23] S.R. Kanel, J.M. Greneche, H. Choi, Arsenic(V) removal from groundwater using nano scale zero-valent iron as a colloidal reactive barrier material, Environ. Sci. Technol. 40 (2006) 2045–2050.
[24] C. Üzüm, T. Shahwan, A.E. Eroglu, I. Lieberwirth, T.B. Scott, K.R. Hallam, Application of zero-valent iron nanoparticles for the removal of aqueous Co^{2+} ions under various experimental conditions, Chem. Eng. J. 144 (2008) 213–220.
[25] C. Clinard, T. Mandalia, D. Tchoubar, F. Bergaya, HRTEM image filtration: nanostructural analysis of a pillared clay, Clays Clay Miner. 51 (2003) 421–429.
[26] P. Yuan, H. He, F. Bergaya, D. Wu, Q. Zhou, J. Zhu, Synthesis and characterization of delaminated iron-pillared clay with meso-microporous structure, Micropor. Mesopor. Mater. 88 (2006) 8–15.
[27] S.A. Bagshaw, T.J. Pinnavaia, Mesoporous alumina molecular sieves, Angew Chem. Int. Ed. Engl. 35 (1996) 1102–1105.
[28] G. Lagaly, S. Ziesmer, Colloid chemistry of clay minerals: the coagulation of montmorillonite dispersions, Adv. Colloid Interface Sci. 100-102 (2003) 105–128.
[29] M.L. Peterson, A.F. White, G.E. Brown, G.A. Parks, Surface passivation of magnetite by reaction with aqueous Cr(VI): XAFS and TEM results, Environ. Sci. Technol. 31 (1997) 1573–1576.
[30] A.R. Pratt, D.W. Blowes, C.J. Ptacek, Products of chromate reduction on proposed subsurface remediation material, Environ. Sci. Technol. 31 (1997) 2492–2498.
[31] A.R. Pratt, N.S. McIntyre, Comments on curve fitting of Cr 2p photoelectron spectra of Cr_2O_3 and CrF_3, Surf. Interface Anal. 24 (1996) 529–530.
[32] D. Park, Y.S. Yun, J.M. Park, XAS and XPS studies on chromium-binding groups of biomaterial during Cr(VI) biosorption, J. Colloid Interface Sci. 317 (2008) 54–61.
[33] K. Asami, K. Hashimoto, An XPS study of the surfaces on Fe–Cr, Fe–Co and Fe–Ni alloys after mechanical polishing, Corros. Sci. 24 (1984) 83–97.
[34] M.L. Werner, P.S. Nico, M.A. Marcus, C. Anastasio, Use of micro-XANES to speciate chromium in airborne fine particles in the sacramento valley, Environ. Sci. Technol. 41 (2007) 4919–4924.
[35] B.A. Manning, J.R. Kiser, H. Kwon, S.R. Kanel, Spectroscopic investigation of Cr(III)- and Cr(VI)-treated nanoscale zerovalent iron, Environ. Sci. Technol. 41 (2006) 586–592.